

Three-flavour neutrino oscillation update

Thomas Schwetz[†], Mariam Tórtola[‡] and José W. F. Valle[§]

[†] Theory Division, Physics Department, CERN CH-1211 Geneva 23, Switzerland

[‡] Departamento de Física and CFTP, Instituto Superior Técnico

Av. Rovisco Pais 1, 1049-001 Lisboa, Portugal

[§] AHEP Group, Instituto de Física Corpuscular – C.S.I.C./Universitat de València, Edificio Institutos de Paterna, Apt 22085, E-46071 Valencia, Spain

E-mail: schwetz@cern.ch, mariam@cftp.ist.utl.pt, valle@ific.uv.es

Abstract. We review the present status of three-flavour neutrino oscillations, taking into account the latest available neutrino oscillation data presented at the *Neutrino 2008* Conference. This includes the data released this summer by the MINOS collaboration, the data of the neutral current counter phase of the SNO solar neutrino experiment, as well as the latest KamLAND and Borexino data. We give the updated determinations of the leading 'solar' and 'atmospheric' oscillation parameters. We find from global data that the mixing angle θ_{13} is consistent with zero within 0.9σ and we derive an upper bound of $\sin^2 \theta_{13} \leq 0.035$ (0.056) at 90% CL (3σ).

Keywords: Neutrino mass and mixing; solar and atmospheric neutrinos; reactor and accelerator neutrinos

PACS numbers: 26.65.+t, 13.15.+g, 14.60.Pq, 95.55.Vj

1. Introduction

Thanks to the synergy amongst a variety of experiments involving solar and atmospheric neutrinos, as well as man-made neutrinos at nuclear power plants and accelerators [1] neutrino physics has undergone a revolution over the last decade or so. The long-sought-for phenomenon of neutrino oscillations has been finally established, demonstrating that neutrino flavor states (ν_e, ν_μ, ν_τ) are indeed quantum superpositions of states (ν_1, ν_2, ν_3) with definite masses m_i [2]. The simplest unitary form of the lepton mixing matrix relating flavor and mass eigenstate neutrinos is given in terms of three mixing angles ($\theta_{12}, \theta_{13}, \theta_{23}$) and three CP-violating phases, only one of which affects (conventional) neutrino oscillations [3]. Here we consider only the effect of the mixing angles in current oscillation experiments, the sensitivity to CP violation effects remains an open challenge for future experiments [4, 5]. Together with the mass splitting parameters $\Delta m_{21}^2 \equiv m_2^2 - m_1^2$ and $\Delta m_{31}^2 \equiv m_3^2 - m_1^2$ the angles θ_{12}, θ_{23} are rather well determined by the oscillation data. In contrast, so far only upper bounds can be placed upon θ_{13} , mainly following from the null results of the short-baseline CHOOZ reactor experiment [6] with some effect also from solar and KamLAND data, especially at low Δm_{31}^2 values [7].

Here we present an update of the three-flavour oscillation analyses of Refs. [7] and [8]. This new analysis includes the data released this summer by the MINOS collaboration [9], the data from the neutral current counter phase of the SNO experiment (SNO-NCD) [10], the latest KamLAND [11] and Borexino [12] data, as well as the results of a recent re-analysis of the Gallex/GNO solar neutrino data presented at the Neutrino 2008 conference [13]. In Section 2 we discuss the status of the parameters relevant for the leading oscillation modes in solar and atmospheric neutrinos. In Section 3 we present the updated limits on θ_{13} and discuss the recent claims for possible hints in favour of a non-zero value made in Refs. [14, 15, 16]. We summarize in Section 4.

2. The leading 'solar' and 'atmospheric' oscillation parameters

Let us first discuss the status of the solar parameters θ_{12} and Δm_{21}^2 . The latest data release from the KamLAND reactor experiment [11] has increased the exposure almost fourfold over previous results [17] to 2.44×10^{32} proton·yr due to longer lifetime and an enlarged fiducial volume, corresponding to a total exposure of 2881 ton·yr. Apart from the increased statistics also systematic uncertainties have been improved: Thanks to the full volume calibration the error on the fiducial mass has been reduced from 4.7% to 1.8%. Details of our KamLAND analysis are described in appendix A of Ref. [8]. We use the data binned in equal bins in $1/E$ to make optimal use of spectral information, we take into account the (small) matter effect and carefully include various systematics following Ref. [18]. As previously, we restrict the analysis to the prompt energy range above 2.6 MeV where the contributions from geo-neutrinos [19] as well as backgrounds are small and the selection efficiency is roughly constant [11]. In that energy range 1549 reactor neutrinos events and a background of 63 events are expected without oscillations,

whereas the observed number of events is 985 [20].

The Sudbury Neutrino Observatory (SNO) has released the data of its last phase, where the neutrons produced in the neutrino NC interaction with deuterium are detected mainly by an array of ^3He proportional counters to measure the rate of neutral-current interactions in heavy water and precisely determine the total active boron solar neutrino flux, yielding the result $5.54_{-0.31}^{+0.33}(\text{stat})_{-0.34}^{+0.36}(\text{syst}) \times 10^6 \text{ cm}^{-2}\text{s}^{-1}$ [10]. The independent ^3He neutral current detectors (NCD) provide a measurement of the neutral current flux uncorrelated with the charged current rate from solar ν_e , different from the statistical CC/NC separation of previous SNO phases. Since the total NC rate receives contributions from the NCD as well as from the PMTs (as previously) a small (anti-) correlation between CC and NC remains. Following Ref. [16] we assume a correlation of $\rho = -0.15$. In our SNO analysis we add the new data on the CC and NC fluxes to the previous results [21] assuming no correlation between the NCD phase and the previous salt phase, see Ref. [7] for further details. The main impact of the new SNO data is due to the lower value for the observed CC/NC ratio, $(\phi_{\text{CC}}/\phi_{\text{NC}})^{\text{NCD}} = 0.301 \pm 0.033$ [10], compared to the previous value $(\phi_{\text{CC}}/\phi_{\text{NC}})^{\text{salt}} = 0.34 \pm 0.038$ [21]. Since for ^8B neutrinos $\phi_{\text{CC}}/\phi_{\text{NC}} \approx P_{ee} \approx \sin^2 \theta_{12}$, adding the new data point on this ratio with the lower value leads to a stronger upper bound on $\sin^2 \theta_{12}$.

We also include the direct measurement of the ^7Be solar neutrino signal rate performed by the Borexino collaboration [12]. They report an interaction rate of the 0.862 MeV ^7Be neutrinos of $49 \pm 3(\text{stat}) \pm 4(\text{syst})$ counts/(day·100 ton). This measurement constitutes the first direct determination of the survival probability for solar ν_e in the transition region between matter-enhanced and vacuum-driven oscillations. The survival probability of 0.862 MeV ^7Be neutrinos is determined to be $P_{ee}^{7\text{Be,obs}} = 0.56 \pm 0.1$. We find that with present errors Borexino plays no significant role in the determination of neutrino oscillation parameters. Apart from the fact that the uncertainty on the survival probability is about a factor 3 larger than e.g., the uncertainty on the SNO CC/NC ratio measurement, it turns out that the observed value for P_{ee} quoted above practically coincides (within 0.1σ) with the prediction at the best fit point: $P_{ee}^{7\text{Be,pred}} = 0.55$.

The new data from SNO and Borexino are combined with the global data on solar neutrinos [22, 23, 24, 25], where we take into account the results of a recent re-analysis of the Gallex data yielding a combined Gallex and GNO rate of $67.6 \pm 4.0 \pm 3.2$ SNU [13].

Fig. 1 illustrates how the determination of the leading solar oscillation parameters θ_{12} and Δm_{21}^2 emerges from the complementarity of solar and reactor neutrinos. From the global three-flavour analysis we find (1σ errors)

$$\sin^2 \theta_{12} = 0.304_{-0.016}^{+0.022}, \quad \Delta m_{21}^2 = 7.65_{-0.20}^{+0.23} \times 10^{-5} \text{ eV}^2. \quad (1)$$

The numerical χ^2 profiles shown in Fig. 1 have to very good accuracy the Gaussian shape $\chi^2 = (x - x_{\text{best}})^2/\sigma^2$, when the different σ for upper and lower branches are used as given in Eq. (1). Spectral information from KamLAND data leads to an accurate determination of Δm_{21}^2 with the remarkable precision of 8% at 3σ , defined

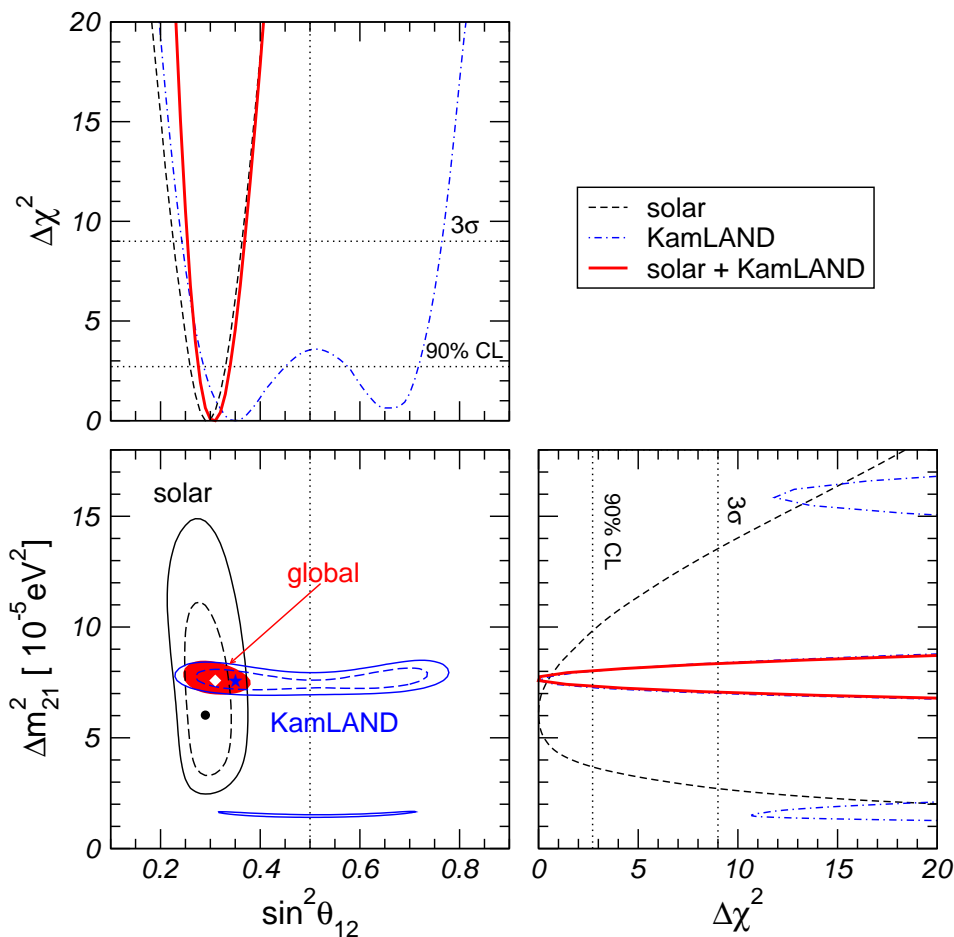


Figure 1. Determination of the leading “solar” oscillation parameters from the interplay of data from artificial and natural neutrino sources. We show χ^2 -profiles and allowed regions at 90% and 99.73% CL (2 dof) for solar and KamLAND, as well as the 99.73% CL region for the combined analysis. The dot, star and diamond indicate the best fit points of solar data, KamLAND and global data, respectively. We minimise with respect to Δm_{31}^2 , θ_{23} and θ_{13} , including always atmospheric, MINOS, K2K and CHOOZ data.

as $(x^{\text{upper}} - x^{\text{lower}})/(x^{\text{upper}} + x^{\text{lower}})$. We find that the main limitation for the Δm_{21}^2 measurement comes from the uncertainty on the energy scale in KamLAND of 1.5%. KamLAND data start also to contribute to the lower bound on $\sin^2 \theta_{12}$, whereas the upper bound is dominated by solar data, most importantly by the CC/NC solar neutrino rate measured by SNO. The SNO-NCD measurement reduces the 3σ upper bound on $\sin^2 \theta_{12}$ from 0.40 [8] to 0.37.

Let us now move to the discussion of the status of the leading atmospheric parameters θ_{23} and Δm_{31}^2 . The Main Injector Neutrino Oscillation Search experiment (MINOS) has reported new results on ν_μ disappearance with a baseline of 735 km based on a two-year exposure from the Fermilab NuMI beam. Their data, recorded between May 2005 and July 2007 correspond to a total of 3.36×10^{20} protons on target (POT) [9], more than doubling the POT with respect to MINOS run I [26], and increasing the

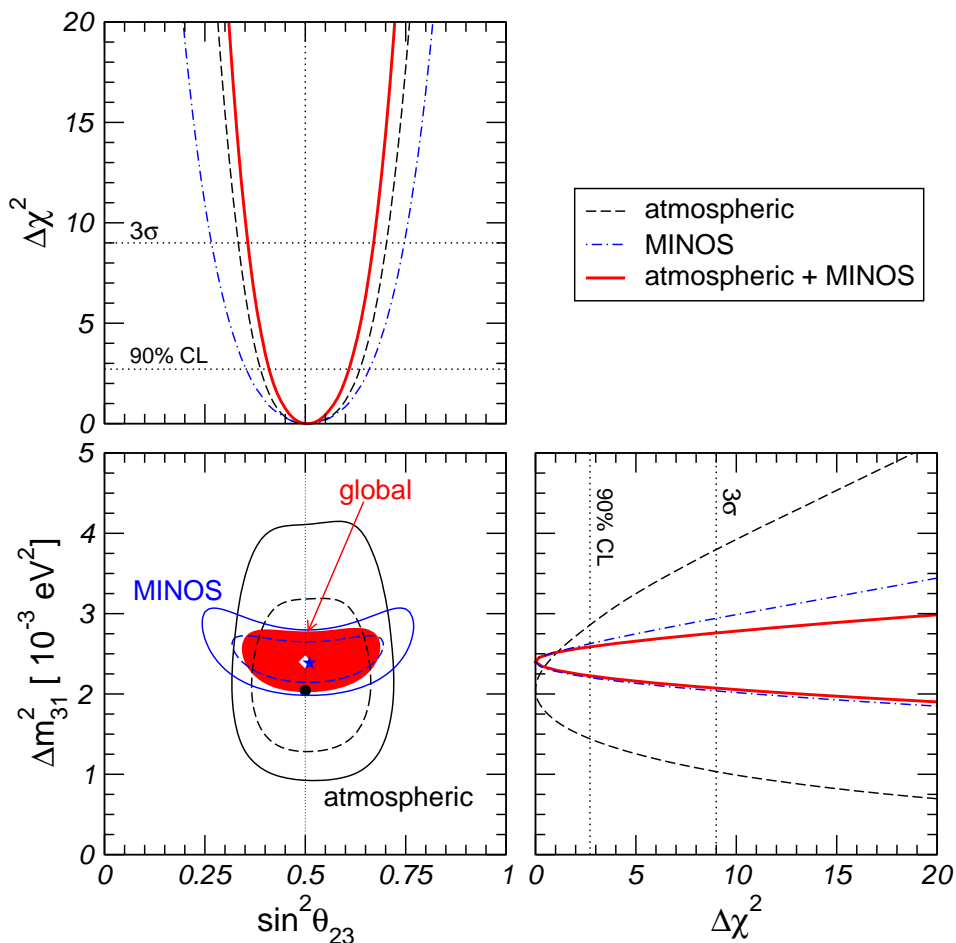


Figure 2. Determination of the leading “atmospheric” oscillation parameters from the interplay of data from artificial and natural neutrino sources. We show χ^2 -profiles and allowed regions at 90% and 99.73% CL (2 dof) for atmospheric and MINOS, as well as the 99.73% CL region for the combined analysis (including also K2K). The dot, star and diamond indicate the best fit points of atmospheric data, MINOS and global data, respectively. We minimise with respect to Δm_{21}^2 , θ_{12} and θ_{13} , including always solar, KamLAND, and CHOOZ data.

exposure used in the latest version of Ref. [8] by about 34%. The latest data confirm the energy dependent disappearance of ν_μ , showing significantly less events than expected in the case of no oscillations in the energy range $\lesssim 6$ GeV, whereas the high energy part of the spectrum is consistent with the no oscillation expectation. We include this result in our analysis by fitting the event spectrum given in Fig. 2 of Ref. [9]. Current MINOS data largely supersedes the pioneering K2K measurement [27] which by now gives only a very minor contribution to the Δm_{31}^2 measurement.

We combine the long-baseline accelerator data with atmospheric neutrino measurements from Super-Kamiokande [28], using the results of Ref. [8], see references therein for details. In this analysis sub-leading effects of Δm_{21}^2 in atmospheric data are neglected, but effects of θ_{13} are included, in a similar spirit as in Ref. [29].

Fig. 2 illustrates how the determination of the leading atmospheric oscillation

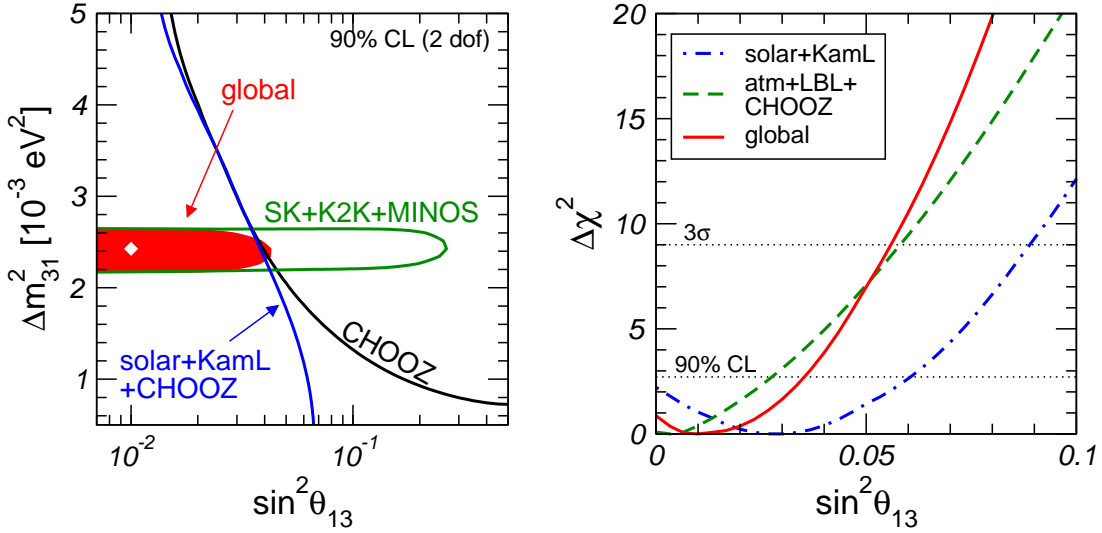


Figure 3. Constraints on $\sin^2 \theta_{13}$ from different parts of the global data.

parameters θ_{23} and $|\Delta m_{31}^2|$ emerges from the complementarity of atmospheric and accelerator neutrino data. We find the following best fit points and 1σ errors:

$$\sin^2 \theta_{23} = 0.50_{-0.06}^{+0.07}, \quad |\Delta m_{31}^2| = 2.40_{-0.11}^{+0.12} \times 10^{-3} \text{ eV}^2. \quad (2)$$

The determination of $|\Delta m_{31}^2|$ is dominated by spectral data from the MINOS long-baseline ν_μ disappearance experiment, where the sign of Δm_{31}^2 (i.e., the neutrino mass hierarchy) is undetermined by present data. The measurement of the mixing angle θ_{23} is still largely dominated by atmospheric neutrino data from Super-Kamiokande with a best fit point at maximal mixing. Small deviations from maximal mixing due to sub-leading three-flavour effects have been found in Refs. [30, 31], see, however, also Ref. [32] for a preliminary analysis of Super-Kamiokande. A comparison of these subtle effects can be found in Ref. [33]. At present deviations from maximality are not statistically significant.

3. Status of θ_{13}

The third mixing angle θ_{13} would characterize the magnitude of CP violation in neutrino oscillations. Together with the determination of the neutrino mass spectrum hierarchy (i.e., the sign of Δm_{31}^2) it constitutes a major open challenge for any future investigation of neutrino oscillations [4, 5].

Fig. 3 summarizes the information on θ_{13} from present data. Similar to the case of the leading oscillation parameters, also the bound on θ_{13} emerges from an interplay of different data sets, as illustrated in the left panel of Fig. 3. An important contribution to the bound comes, of course, from the CHOOZ reactor experiment [6] combined with the determination of $|\Delta m_{31}^2|$ from atmospheric and long-baseline experiments. Due to a complementarity of low and high energy solar neutrino data, as well as solar and

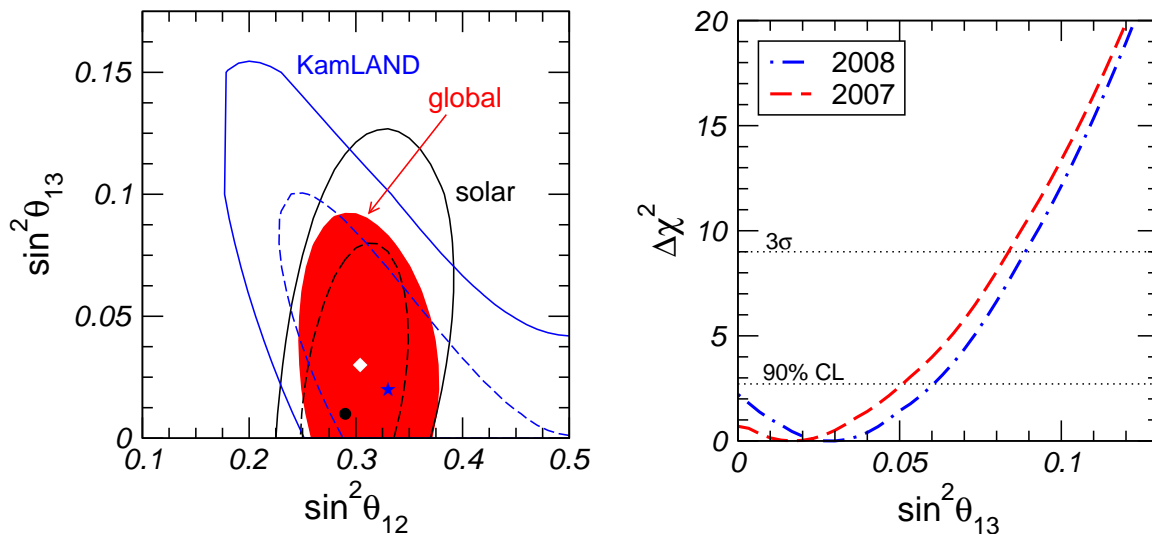


Figure 4. Left: Allowed regions in the $(\theta_{12} - \theta_{13})$ plane at 90% and 99.73% CL (2 dof) for solar and KamLAND, as well as the 99.73% CL region for the combined analysis. Δm_{21}^2 is fixed at its best fit point. The dot, star, and diamond indicate the best fit points of solar, KamLAND, and combined data, respectively. Right: χ^2 profile from solar and KamLAND data with and without the 2008 SNO-NCD data.

KamLAND data, one finds that also solar+KamLAND provide a non-trivial constraint on θ_{13} , see e.g., Refs. [7, 8] [34]. We obtain at 90% CL (3σ) the following limits ‡:

$$\sin^2 \theta_{13} \leq \begin{cases} 0.060 (0.089) & (\text{solar+KamLAND}) \\ 0.027 (0.058) & (\text{CHOOZ+atm+K2K+MINOS}) \\ 0.035 (0.056) & (\text{global data}) \end{cases} \quad (3)$$

In the global analysis we find a slight weakening of the upper bound on $\sin^2 \theta_{13}$ due to the new data from 0.04 (see Ref. [33] or v5 of [8]) to 0.056 at 3σ . The reason for this is two-fold. First, the shift of the allowed range for $|\Delta m_{31}^2|$ to lower values due to the new MINOS data implies a slightly weaker constraint on $\sin^2 \theta_{13}$ (cf. Fig. 3, left), and second, the combination of solar and new KamLAND data prefers a slightly non-zero value of $\sin^2 \theta_{13}$ which, though not statistically significant, also results in a weaker constraint in the global fit (cf. Fig. 3, right).

As has been noted in Ref. [16] the slight downward shift of the SNO CC/NC ratio due to the SNO-NCD data leads to a “hint” for a non-zero value of θ_{13} . From the combination of solar and KamLAND data we find a best fit value of $\sin^2 \theta_{13} = 0.03$ with $\Delta\chi^2 = 2.2$ for $\theta_{13} = 0$ which corresponds to a 1.5σ effect (86% CL). We illustrate the interplay of solar and KamLAND data in the left panel of Fig. 4. The survival probability in KamLAND is given by

$$P_{ee}^{\text{KamL}} \approx \cos^4 \theta_{13} \left(1 - \sin^2 2\theta_{12} \sin^2 \frac{\Delta m_{21}^2 L}{4E} \right), \quad (4)$$

‡ Note that the bounds given in Eq. (3) are obtained for 1 dof, whereas in Fig. 3 (left) the 90% CL regions for 2 dof are shown.

leading to an anti-correlation of $\sin^2 \theta_{13}$ and $\sin^2 \theta_{12}$ [8], see also [14, 34]. In contrast, for solar neutrinos one has

$$P_{ee}^{\text{solar}} \approx \begin{cases} \cos^4 \theta_{13} \left(1 - \frac{1}{2} \sin^2 2\theta_{12}\right) & \text{low energies} \\ \cos^4 \theta_{13} \sin^2 \theta_{12} & \text{high energies} \end{cases} . \quad (5)$$

Eq. (5) shows a similar anti-correlation as in KamLAND for the vacuum oscillations of low energy solar neutrinos. For the high energy part of the spectrum, which undergoes the adiabatic MSW conversion inside the sun and which is subject to the SNO CC/NC measurement, a positive correlation of $\sin^2 \theta_{13}$ and $\sin^2 \theta_{12}$ emerges. As visible from Fig. 4 (left) and as discussed already in Refs. [8, 34], this complementarity leads to a non-trivial constraint on θ_{13} and it allows to understand the hint for a non-zero value of θ_{13} , which helps to reconcile the slightly different best fit points for θ_{12} for solar and KamLAND separately [14, 16]. This trend was visible already in pre-SNO-NCD data, though with a significance of only 0.8σ , see Fig. 4 (right) showing the present result together with our previous one from v6 of [8].

Let us briefly comment on a possible additional hint for a non-zero θ_{13} from atmospheric neutrino data [15, 30]; Refs. [16, 30] find from atmospheric+long-baseline+CHOOZ data a 0.9σ hint for a non-zero value: $\sin^2 \theta_{13} = 0.012 \pm 0.013$. In our atmospheric neutrino analysis (neglecting Δm_{21}^2 effects) combined with CHOOZ data the best fit occurs for $\theta_{13} = 0$ (cf. Fig. 3, right), in agreement with Ref. [29]. Also, in the atmospheric neutrino analysis from Ref. [31] (which does include Δm_{21}^2 effects, as Refs. [16, 30]) the preference for a non-zero θ_{13} is much weaker than the one from [30], with a $\Delta\chi^2 \lesssim 0.2$. In our global analysis the hint from solar+KamLAND gets diluted by the constraint coming from atmospheric+CHOOZ data, and we find the global χ^2 minimum at $\sin^2 \theta_{13} = 0.01$, but with $\theta_{13} = 0$ allowed at 0.9σ ($\Delta\chi^2 = 0.87$). Hence, we conclude that at present there is no significant hint for a non-zero θ_{13} . As already stated, the origin of slightly different conclusions of other studies is related with including or neglecting the effect of solar terms in the atmospheric neutrino oscillation analysis, and translates also into a possibly nonmaximal best fit value for θ_{23} . Note, however, that all analyses agree within $\Delta\chi^2$ values of order 1 and therefore there is no significant disagreement. A critical discussion of the impact of sub-leading effects in atmospheric data on θ_{13} and θ_{23} as well as a comparison of the results of different groups can be found in Ref. [33].

Before summarizing let us update also the determination of the ratio of the two mass-squared differences,

$$\alpha \equiv \frac{\Delta m_{21}^2}{|\Delta m_{31}^2|} = 0.032, \quad 0.027 \leq \alpha \leq 0.038 \quad (3\sigma), \quad (6)$$

which is relevant for the description of CP violation in neutrino oscillations in long-baseline experiments.

4. Summary

In this work we have provided an update on the status of three-flavour neutrino oscillations, taking into account the latest available world neutrino oscillation data presented at the *Neutrino 2008* Conference. Our results are summarized in Figures 1, 2 and 3. Table 1 provides best fit points, 1σ errors, and the allowed intervals at 2 and 3σ for the three-flavour oscillation parameters.

parameter	best fit	2σ	3σ
Δm_{21}^2 [10^{-5}eV^2]	$7.65^{+0.23}_{-0.20}$	7.25–8.11	7.05–8.34
$ \Delta m_{31}^2 $ [10^{-3}eV^2]	$2.40^{+0.12}_{-0.11}$	2.18–2.64	2.07–2.75
$\sin^2 \theta_{12}$	$0.304^{+0.022}_{-0.016}$	0.27–0.35	0.25–0.37
$\sin^2 \theta_{23}$	$0.50^{+0.07}_{-0.06}$	0.39–0.63	0.36–0.67
$\sin^2 \theta_{13}$	$0.01^{+0.016}_{-0.011}$	≤ 0.040	≤ 0.056

Table 1. Best-fit values with 1σ errors, and 2σ and 3σ intervals (1 d.o.f.) for the three-flavour neutrino oscillation parameters from global data including solar, atmospheric, reactor (KamLAND and CHOOZ) and accelerator (K2K and MINOS) experiments.

Acknowledgments. This work was supported by MEC grant FPA2005-01269, by EC Contracts RTN network MRTN-CT-2004-503369 and ILIAS/N6 RII3-CT-2004-506222. We thank Michele Maltoni for collaboration on global fits to neutrino oscillation data.

Appendix A. Updated analysis as of February 2010

Appendix A.1. Updates in the solar neutrino analysis

SSM: We consider the recently updated standard solar model from [35]. Among the different models presented in that reference, we use the low metallicity model, labelled as AGSS09, that incorporates the most recent determination of solar abundances [36] as our standard choice. The solar abundances in that model are a bit higher than previous determinations by the same group, alleviating the disagreement with helioseismic data. From the point of view of solar neutrinos, the most important changes with respect to the previous SSM used in our analysis (BS05(OP), with high metallicities [37]) is the 15% and 5% reduction in the Boron and Beryllium fluxes respectively. This is due to the reduced central temperature in the new model with respect to the previous one. Given the condition of fixed solar luminosity, this reduction is compensated by a slight increase in the pp and pep neutrino fluxes. We discuss also the impact of a new SSM with high metallicity, the GS98 model (presented in [35] as well), see also the recent discussion in [38].

SAGE: In our present analysis we have updated the capture rate of solar neutrinos measured in SAGE: $65.4_{-3.0-2.8}^{+3.1+2.6}$ SNU [39], compared to the previous value $66.9_{-3.8-3.2}^{+3.9+3.6}$ SNU [40]. Note that the recently published reanalysis of GALLEX data [41] has been reported already at Neutrino 2008 [13] and was therefore included in the original version of this paper.

SNO: In our update we include also the results from the recent joint re-analysis of data from the Phase I and Phase II (the pure D₂O and salt phases) of the Sudbury Neutrino Observatory (SNO) [42]. In this analysis, an effective electron kinetic energy threshold of 3.5 MeV has been used (Low Energy Threshold Analysis, LETA), and the total flux of ⁸B neutrinos has been determined to be

$$\phi_{NC} = 5.140_{-0.158}^{+0.160}(\text{stat})_{-0.117}^{+0.132}(\text{syst}) \times 10^6 \text{ cm}^{-2} \text{ s}^{-1}. \quad (\text{A.1})$$

Comparing this number with the result obtained in SNO Phase III (the NC detector phase, NCD): $5.54_{-0.31}^{+0.33}(\text{stat})_{-0.34}^{+0.36}(\text{syst}) \times 10^6 \text{ cm}^{-2} \text{ s}^{-1}$ [10], one can see that the determination of the total neutrino flux has been improved by about a factor 2. These improvements have been possible thanks mainly to the increased statistics, in particular the NC event sample in the LETA is increased by about 70%, since the previously used higher energy thresholds of 5 MeV in phase I and 5.5 MeV in phase II have cut away a significant portion of the NC events. Furthermore, energy resolution, backgrounds suppression, and systematic uncertainties have been improved. We include the LETA SNO data by fitting the predicted energy-dependent neutrino survival probability and day-night asymmetry in terms of the polynomials given by the SNO collaboration, see Tabs. XXVI and XXVII in [42]. We have checked that our results agree with the analysis including all solar neutrino experiments made by SNO. Note that we have adopted in our present analysis of the SNO-NCD phase data the detailed correlations between the CC, NC and ES neutrino fluxes recently given by the SNO collaboration [43], thereby improving our previous treatment presented in Sec. 2.

Fig. A1 shows the impact of the updates in the solar analysis on the determination of the solar parameters. The left panel compares solar and solar+KamLAND allowed regions for the previous and updated analyses, the middle panel illustrates the impact of the SNO LETA analysis, and the right panel shows the effect of changing between the low (AGSS09) and high (GS98) metallicity solar models. We observe that the main changes come from the SNO LETA analysis, whereas the impact of solar metallicity is small. In general changes are rather small, once KamLAND data is added to the solar data, with a small tightening of the lower bound on $\sin^2 \theta_{12}$. The best fit point value for the solar mixing angle has been shifted to a slightly higher value mainly due to the lower values reported for the total boron neutrino flux, either from the SNO LETA measurements as well as from the updated SSM with low metallicities. The allowed range for Δm_{21}^2 of solar only data has been somewhat reduced, however this effect gets completely diluted after combining with KamLAND data. The updated best fit values and allowed ranges for $\sin^2 \theta_{12}$ and Δm_{21}^2 can be found in Tab. A1.

The impact of the updated solar analysis on θ_{13} is illustrated in Fig. A2. Our

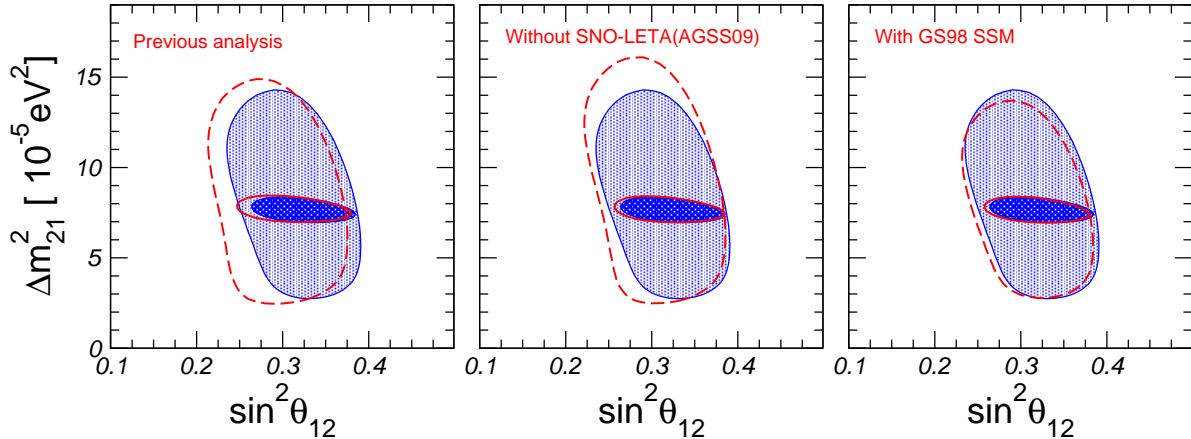


Figure A1. Impact of the changes in the solar neutrino analysis. In all panels the blue (shaded) regions corresponds to the 3σ regions from solar and solar+KamLAND updated analysis. The regions delimited by the red contour curves correspond to our previous analysis (left), an analysis using the previous high-threshold SNO phase I and II analysis but the same solar model (middle), and an analysis using the high metallicity GS98 instead of our standard low metallicity AGSS09 solar model (right).

analysis of solar + KamLAND data gives $\sin^2\theta_{13} = 0.022_{-0.015}^{+0.018}$ in excellent agreement with the value obtained by the SNO Collaboration [42], $\sin^2\theta_{13} = 0.0200_{-0.0163}^{+0.0209}$. Hence, we obtain a lower best fit value with respect to the one we obtained in our previous analysis ($\sin^2\theta_{13} = 0.03$). This is due to the fact that now solar data prefer a somewhat higher value of θ_{12} (as KamLAND does), and therefore, a smaller value of θ_{13} is required to reconcile solar and KamLAND data, as can be seen by comparing left panels of Figs. 4 and A2. The fact that now solar data prefer a larger value for $\sin^2\theta_{12}$ results in a stronger bound on θ_{13} from the combination of solar + KamLAND data. The allowed solar region in the panel $(\sin^2\theta_{12}, \sin^2\theta_{13})$ is more shifted to the right (because of the higher θ_{12} preferred by the new smaller boron neutrino flux), where the allowed KamLAND region is narrower. At $\theta_{13} = 0$ we find $\Delta\chi^2 = 2.2$, same value as before.

As stated above, the small improvement in the θ_{13} bound is related to the solar model used. For models with higher solar metallicities like GS98, a slightly weaker bound is obtained [38], see Fig. A2 (right). In that case we obtain a slightly larger best fit point, $\sin^2\theta_{13} = 0.027_{-0.015}^{+0.019}$ and $\Delta\chi^2 = 3.05$ at $\theta_{13} = 0$.

Appendix A.2. MINOS ν_e appearance data

In Ref. [44] a search for $\nu_\mu \rightarrow \nu_e$ transitions by the MINOS experiment has been presented, based on a 3.14×10^{20} protons-on-target exposure in the Fermilab NuMI beam. 35 events have been observed in the far detector with a background of $27 \pm 5(\text{stat}) \pm 2(\text{syst})$ events predicted by the measurements in the near detector. This corresponds to an excess of about 1.5σ which can be interpreted as a weak hint for ν_e appearance due to a non-zero θ_{13} . We fit the MINOS ν_e spectrum by using the GLOBES simulation software [45], where we calibrate our predicted spectrum by using

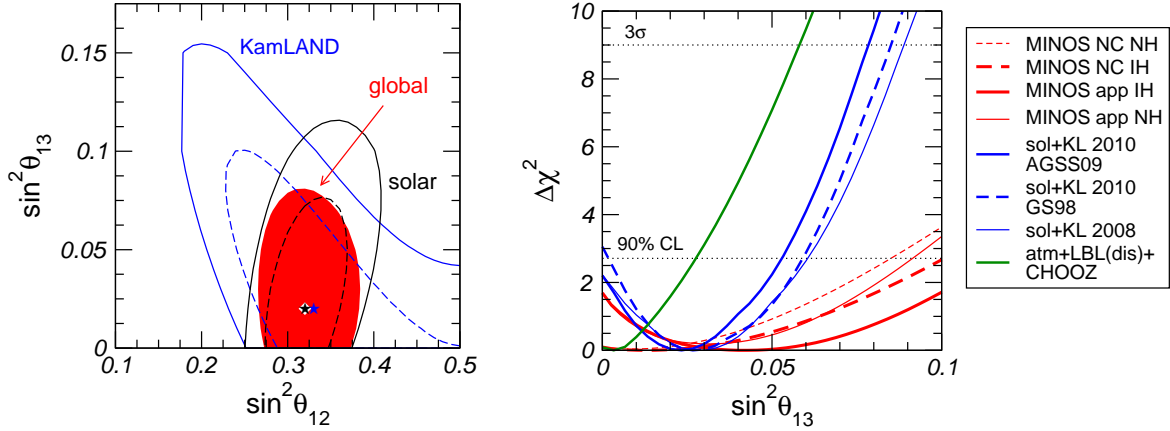


Figure A2. Left (update of Fig. 4, left): Allowed regions in the $(\theta_{12} - \theta_{13})$ plane at 90% and 99.73% CL (2 dof) for solar and KamLAND, as well as the 99.73% CL region for the combined analysis. Right: $\Delta\chi^2$ as a function of $\sin^2 \theta_{13}$. The blue curves illustrate the impact of the updates in the solar neutrino analysis on the bound from the global solar+KamLAND data. The red curves show the constraint coming from the MINOS ν_e appearance (red solid) and NC (red dashed) data, where we show the $\Delta\chi^2$ assuming NH (thin) and IH (thick), both with respect to the common minimum, which occurs for IH. The green solid curve corresponds the bound from CHOOZ + atmospheric + K2K + MINOS (disappearance) data.

the information given in [46]. A full three-flavour fit is performed taking into account a 7.3% uncertainty on the background normalization (Tab. I of [44]), and a 5% uncertainty on the matter density along the neutrino path.

In the MINOS detector, being optimized for muons, it is rather difficult to identify ν_e CC events, since they lead to an electromagnetic shower. NC and ν_μ CC events often have a similar signature, and hence lead to a background for the ν_e appearance search. Indeed, in Ref. [47] an analysis of “NC events” has been performed, where “NC events” in fact include also ν_e CC events due to the similar event topology. Therefore, a possible $\nu_\mu \rightarrow \nu_e$ oscillation signal would contribute to the “NC event” sample of [47] and these data can be used to constrain θ_{13} . We have performed a fit to the observed spectrum, again using the GLOBES software, by summing the NC events induced from the total neutrino flux with the ν_e CC appearance signal due to oscillations. We include a 4% error on the predicted NC spectrum and a 3% error on the ν_μ CC induced background (Tab. II of [47]).

In Fig. A2 (right) we show the constraint on $\sin^2 \theta_{13}$ from these MINOS data. The χ^2 has been marginalized with respect to all parameters except θ_{13} , where for the solar and atmospheric parameters we imposed Gaussian errors taken from Tab. A1, without including any other information on θ_{13} except from MINOS. We show the $\Delta\chi^2$ profiles for ν_e appearance data and NC data, for a fixed neutrino mass hierarchy. The best fit point is always obtained for the inverted hierarchy (IH, $\Delta m_{31}^2 < 0$), and in that case in general the constraint on $\sin^2 \theta_{13}$ is weaker, since for IH the matter effect tends to suppress the ν_e appearance probability. The $\Delta\chi^2$ for normal hierarchy (NH, $\Delta m_{31}^2 > 0$)

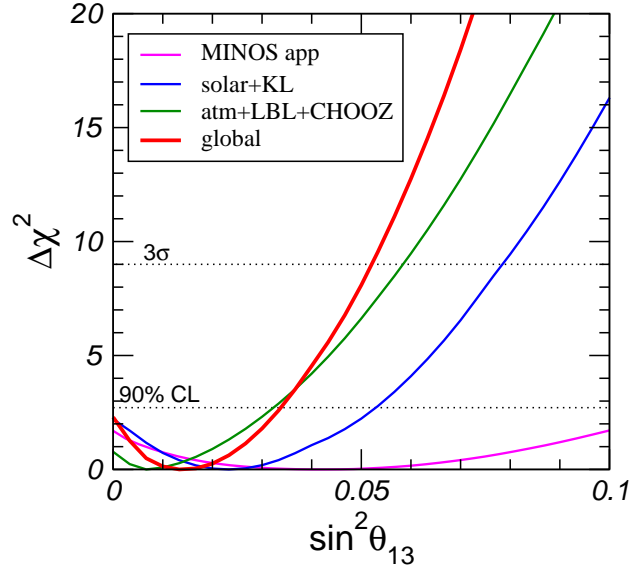


Figure A3. The constraint on $\sin^2 \theta_{13}$ from MINOS ν_e appearance data, solar + KamLAND data, atmospheric + CHOOZ + K2K + MINOS (disappearance as well as appearance), and the combined global data.

is given with respect to the best fit for IH. In the global analysis we also marginalize over the two hierarchies, and hence, the actual information from MINOS comes from the IH.

We see from the figure that MINOS ν_e appearance data shows a slight preference for a non-zero value of θ_{13} , with a best fit point of $\sin^2 \theta_{13} = 0.032(0.043)$ for NH (IH) with $\Delta\chi^2 = 1.8$ at $\sin^2 \theta_{13} = 0$. In contrast, no indication for a non-zero θ_{13} comes from the NC data. Furthermore, one observes that NC gives a slightly more constraining upper bound on $\sin^2 \theta_{13}$ than ν_e appearance, while both are significantly weaker than the bound from ν_μ disappearance data + CHOOZ or solar+KamLAND. Let us mention that the result for the NC analysis strongly depends on the value assumed for the systematic uncertainty, whereas the ν_e appearance result is more robust with respect to systematics, being dominated by statistics.

In the global analysis we do not combine the χ^2 's from MINOS ν_e and NC data, since presumably the data are not independent and adding them would imply a double counting of the same data. Therefore, we adopt the conservative approach and use only ν_e appearance data without the information from NC data in the global analysis. We have checked, however, that adding both MINOS data sets leads to practically the same result in the global fit, both for the “hint” for $\theta_{13} > 0$ as well as the global bound, the latter being dominated by other data sets.

Appendix A.3. Updated global three-flavour fit

The present situation on the mixing angle θ_{13} is summarized in Fig. A3. We obtain the following bounds at 90% (3σ) CL:

$$\sin^2 \theta_{13} \leq \begin{cases} 0.053 \text{ (0.078)} & \text{(solar+KamLAND)} \\ 0.033 \text{ (0.061)} & \text{(CHOOZ+atm+K2K+MINOS)} \\ 0.034 \text{ (0.053)} & \text{(global data)} \end{cases} \quad (\text{A.2})$$

We note a slight tightening of the bounds from solar+KamLAND as well as the global bound, due to the update in the solar analysis, see Appendix A.1, whereas the bound from CHOOZ+atm+K2K+MINOS gets slightly weaker, due to MINOS appearance data. In the global analysis we obtain the following best fit value and 1σ range:

$$\sin^2 \theta_{13} = 0.013_{-0.009}^{+0.013} \quad (\text{A.3})$$

This corresponds to a 1.5σ hint for $\theta_{13} > 0$ ($\Delta\chi^2 = 2.3$ at $\theta_{13} = 0$). As discussed in sec. 3 above, in our previous analysis the 1.5σ hint for $\theta_{13} > 0$ from solar+KamLAND data was diluted after the combination with atmospheric, long-baseline and CHOOZ data, resulting in a combined effect of 0.9σ . Now, thanks to the new MINOS appearance data, we find that the atmospheric + long-baseline + CHOOZ analysis already gives a nonzero best fit value of θ_{13} (see Fig. A3), leading to the above global result, eq. A.3.

Finally, let us comment on the possible hint for a non-zero θ_{13} from atmospheric data [16, 30], as discussed in sec. 3. The possible origin of such a hint has been investigated in Ref. [48] and recently in [38], see also [49]. From these results one may conclude that the statistical relevance of the claimed hint for non-zero θ_{13} from atmospheric data depends strongly on the details of the rate calculations and of the χ^2 analysis. Furthermore, the origin of that effect might be traced back to a small excess (at the 1σ level) in the multi-GeV e -like data sample in SK-I, which however, is no longer present in the combined SK-I and SK-II, as well as SK-I+II+III data.

parameter	best fit	2σ	3σ
Δm_{21}^2 [10^{-5}eV^2]	$7.59_{-0.18}^{+0.23}$	7.22–8.03	7.03–8.27
$ \Delta m_{31}^2 $ [10^{-3}eV^2]	$2.40_{-0.11}^{+0.12}$	2.18–2.64	2.07–2.75
$\sin^2 \theta_{12}$	$0.318_{-0.016}^{+0.019}$	0.29–0.36	0.27–0.38
$\sin^2 \theta_{23}$	$0.50_{-0.06}^{+0.07}$	0.39–0.63	0.36–0.67
$\sin^2 \theta_{13}$	$0.013_{-0.009}^{+0.013}$	≤ 0.039	≤ 0.053

Table A1. Current update of Tab. 1: Best-fit values with 1σ errors, and 2σ and 3σ intervals (1 d.o.f.) for the three-flavour neutrino oscillation parameters from global data including solar, atmospheric, reactor (KamLAND and CHOOZ) and accelerator (K2K and MINOS) experiments.

Tab. A1 gives an updated summary of the present best fit values and allowed ranges for the three-flavor oscillation parameters.

References

- [1] For recent reviews see Talks by H. Robertson, P. Decowski, H. Gallagher, C. Galbiati at the *Neutrino 2008* Conference.
<http://www2.phys.canterbury.ac.nz/~jaa53/>
- [2] C. Amsler et al. Review of particle physics. *Phys. Lett.*, B667:1, 2008.
- [3] J. Schechter and J. W. F. Valle. Neutrino masses in $su(2) \times u(1)$ theories. *Phys. Rev.*, D22:2227, 1980; D23:1666, 1981.
- [4] A. Bandyopadhyay et al. Physics at a future Neutrino Factory and super-beam facility. arXiv:0710.4947 [hep-ph].
- [5] H. Nunokawa, S. J. Parke, and J. W. F. Valle. CP Violation and Neutrino Oscillations. *Prog. Part. Nucl. Phys.*, 60:338–402, 2008.
- [6] M. Apollonio et al. Search for neutrino oscillations on a long base-line at the CHOOZ nuclear power station. *Eur. Phys. J.*, C27:331–374, 2003.
- [7] M. Maltoni, T. Schwetz, M. A. Tortola, and J. W. F. Valle. Status of three-neutrino oscillations after the SNO-salt data. *Phys. Rev.*, D68:113010, 2003.
- [8] M. Maltoni, T. Schwetz, M. A. Tortola, and J. W. F. Valle. Status of global fits to neutrino oscillations. *New J. Phys.*, 6:122, 2004. In its arXiv version [hep-ph/0405172v6] this review provides results updated as of September 2007.
- [9] P. Adamson et al. Measurement of Neutrino Oscillations with the MINOS Detectors in the NuMI Beam. arXiv:0806.2237 [hep-ex].
- [10] B. Aharmim et al. An Independent Measurement of the Total Active 8B Solar Neutrino Flux Using an Array of ^3He Proportional Counters at the Sudbury Neutrino Observatory. *Phys. Rev. Lett.*, 101:111301, 2008 [arXiv:0806.0989].
- [11] S. Abe et al. Precision Measurement of Neutrino Oscillation Parameters with KamLAND. *Phys. Rev. Lett.*, 100:221803, 2008. arXiv:0801.4589 [hep-ex].
- [12] The Borexino Collaboration. New results on solar neutrino fluxes from 192 days of Borexino data. arXiv:0805.3843 [astro-ph].
- [13] R. L. Hahn. Talk at the *Neutrino 2008* Conference.
- [14] A. B. Balantekin and D. Yilmaz. Contrasting solar and reactor neutrinos with a non-zero value of θ_{13} . *J. Phys.*, G35:075007, 2008 [arXiv:0804.3345].
- [15] J. Escamilla, D. C. Latimer, and D. J. Ernst. Atmospheric neutrino oscillation data constraints on θ_{13} . arXiv:0805.2924 [nucl-th].
- [16] G. L. Fogli, E. Lisi, A. Marrone, A. Palazzo, and A. M. Rotunno. Hints of $\theta_{13} > 0$ from global neutrino data analysis. arXiv:0806.2649 [hep-ph].
- [17] T. Araki et al. Measurement of neutrino oscillation with KamLAND: Evidence of spectral distortion. *Phys. Rev. Lett.* 94:081801, 2005 [arXiv:hep-ex/0406035].
- [18] P. Huber and T. Schwetz. Precision spectroscopy with reactor anti-neutrinos. *Phys. Rev.* D70:053011, 2004 [arXiv:hep-ph/0407026].

- [19] J. Learned. Talk at the *Neutrino 2008* Conference.
- [20] I. Shimizu. Talk at the *TAUP 2007* Conference.
- [21] B. Aharmim et al. Electron energy spectra, fluxes, and day-night asymmetries of B-8 solar neutrinos from the 391-day salt phase SNO data set. *Phys. Rev. C*72:055502, 2005 [arXiv:nucl-ex/0502021].
- [22] B. T. Cleveland et al. Measurement of the solar electron neutrino flux with the Homestake chlorine detector. *Astrophys. J.* 496:505, 1998.
- [23] J.N. Abdurashitov et al. Measurement of the solar neutrino capture rate by the Russian-American gallium solar neutrino experiment during one half of the 22-year cycle of solar activity. *J. Exp. Theor. Phys.* 95:181, 2002 [astro-ph/0204245].
- [24] M. Altmann et al. Complete results for five years of GNO solar neutrino observations. *Phys. Lett. B*616:174, 2005 [hep-ex/0504037].
- [25] J. Hosaka et al. Solar neutrino measurements in Super-Kamiokande-I. *Phys. Rev. D*73:112001, 2006 [hep-ex/0508053].
- [26] D. G. Michael et al. Observation of muon neutrino disappearance with the MINOS detectors and the NuMI neutrino beam. *Phys. Rev. Lett.*, 97:191801, 2006.
- [27] E. Aliu et al. Evidence for muon neutrino oscillation in an accelerator-based experiment. *Phys. Rev. Lett.*, 94:081802, 2005.
- [28] Y. Ashie et al. A measurement of atmospheric neutrino oscillation parameters by Super-Kamiokande I. *Phys. Rev.*, D71:112005, 2005.
- [29] J. Hosaka et al. Three flavor neutrino oscillation analysis of atmospheric neutrinos in Super-Kamiokande. *Phys. Rev. D*74:032002, 2006 [arXiv:hep-ex/0604011].
- [30] G. L. Fogli, E. Lisi, A. Marrone and A. Palazzo. Global analysis of three-flavor neutrino masses and mixings. *Prog. Part. Nucl. Phys.* 57:742, 2006 [arXiv:hep-ph/0506083].
- [31] M. C. Gonzalez-Garcia and M. Maltoni. Phenomenology with Massive Neutrinos. *Phys. Rept.*, 460:1–129, 2008 [arXiv:0704.1800].
- [32] T. Kajita. Talk at the *NuFact05* Conference.
http://www.lnf.infn.it/conference/nufact05/talks2/WG1/Kajita_WG1.ppt
- [33] T. Schwetz. Global fits to neutrino oscillation data. *Phys. Scripta*, T127:1, 2006. Talk at the *SNOW 2006* Workshop.
<http://www.theophys.kth.se/snow2006/060502/01-schwetz.pdf>
- [34] S. Goswami and A. Yu. Smirnov. Solar neutrinos and 1-3 leptonic mixing. *Phys. Rev.*, D72:053011, 2005.
- [35] Aldo Serenelli, Sarbani Basu, Jason W. Ferguson, and Martin Asplund. New Solar Composition: The Problem With Solar Models Revisited. arXiv:0909.2668.
- [36] Martin Asplund, Nicolas Grevesse, A. Jacques Sauval, and Pat Scott. The chemical composition of the Sun. *Ann. Rev. Astron. Astrophys.*, 47:481–522, 2009 [arXiv:0909.0948].

- [37] John N. Bahcall, Aldo M. Serenelli, and Sarbani Basu. New solar opacities, abundances, helioseismology, and neutrino fluxes. *Astrophys. J.*, 621:L85–L88, 2005 [astro-ph/0412440].
- [38] M. C. Gonzalez-Garcia, Michele Maltoni, and Jordi Salvado. Updated global fit to three neutrino mixing: status of the hints of $\theta_{13} > 0$. arXiv:1001.4524.
- [39] J. N. Abdurashitov et al. Measurement of the solar neutrino capture rate with gallium metal. III: Results for the 2002–2007 data-taking period. *Phys. Rev.*, C80:015807, 2009.
- [40] C. Cattadori. Results from radiochemical solar neutrino experiments. Talk at 21st Int. Conf. on Neutrino Physics and Astrophysics (Paris, June 2004).
- [41] F. Kaether, W. Hampel, G. Heusser, J. Kiko and T. Kirsten. Reanalysis of the GALLEX solar neutrino flux and source experiments. arXiv:1001.2731.
- [42] The SNO Collaboration. Low Energy Threshold Analysis of the Phase I and Phase II Data Sets of the Sudbury Neutrino Observatory. arXiv:0910.2984.
- [43] SNO Collaboration. Physics Interpretation Working Group. HOWTO use the SNO NCD Flux Results.
http://www.sno.phy.queensu.ca/sno/papers/ncd_chi2/howto.pdf.
- [44] The MINOS Collaboration. P. Adamson et al. Search for muon-neutrino to electron-neutrino transitions in MINOS. *Phys. Rev. Lett.* 103:261802 (2009) [arXiv:0909.4996].
- [45] P. Huber, J. Kopp, M. Lindner, M. Rolinec and W. Winter. New features in the simulation of neutrino oscillation experiments with GLOBES 3.0. *Comput. Phys. Commun.* 177:432 (2007) [hep-ph/0701187].
- [46] J. A. A. Boehm. Measurement of electron neutrino appearance with the MINOS experiment. FERMILAB-THESIS-2009-17.
- [47] The MINOS Collaboration. P. Adamson et al. Search for active neutrino disappearance using neutral-current interactions in the MINOS long-baseline experiment. *Phys. Rev. Lett.* 101:221804 (2008) [arXiv:0807.2424].
- [48] M. Maltoni and T. Schwetz. Three-flavour neutrino oscillation update and comments on possible hints for a non-zero θ_{13} . arXiv:0812.3161.
- [49] G. L. Fogli, E. Lisi, A. Marrone, A. Palazzo and A. M. Rotunno. SNO, KamLAND and neutrino oscillations: θ_{13} . arXiv:0905.3549.